Supporting Information

Dual-Site Molecular Passivation at the Buried Interface for High-Efficiency and Stable Perovskite Solar Cells

Yi Dong, Houru Zhu, Ting Zhu, Yuzhu Guo, Jing Zhuang, Yaru Li, Chenhui Zhang, Fangtian Yo, Chunjun Liang and Guitao Feng.

Experimental details

Materials

PbI_2 (99.99%), $HC(NH_2)_2I$ (FAI, 99.5%), CsI (99.5%), Methylammonium iodide (MAI), Lead(II) Bromide ($PbBr_2$, 98%), 4-(3,6-dimethyl-9H-carbazole-9-yl) butyl) phosphonic acid (Me-4PACz) were purchased from TCI; 3,5-Dimethyl-1-pyrazolylformamidinium nitrate (DPN, 97%) from Macklin; NiO_X, [6,6]-phenyl-C61-butyric acid methyl ester (PCBM) and Fullerene (C60) from Liaoning Youxuan Technology; zirconium acetylacetonate ($Zr(acac)_4$) from Sigma-Aldrich. All solvents, anhydrous dimethyl sulfoxide (DMSO, extra dry), N, N-dimethylformamide (DMF, extra dry), chlorobenzene and isopropanol (IPA) were purchased from Acros.

Device fabrication

ITO/glass substrates were sequentially cleaned using detergent, deionized water, and ethanol under ultrasonication, followed by ultraviolet ozone treatment for 20 minutes. The charge transport layers were prepared in a fume hood. NiO_X was dissolved in deionized water at a concentration of 10 mg/mL and spin-coated onto ITO substrates at 2000 rpm for 30 s. After that, the substrates were transferred into a nitrogen-filled glovebox, and all subsequent fabrication steps were carried out under inert conditions. Me-4PACz was dissolved in ethanol at 0.5 mg/mL and spin-coated on the NiO_X layer at 4000 rpm for 30 s, followed by annealing at 100°C for 10 minutes. For DPN-modified

devices, DPN was dissolved in DMF at a concentration of 2 mg/mL and spin-coated onto the Me-4PACz layer at 5000 rpm for 30 s. For control devices, this step was omitted. The perovskite precursor solution of $Cs_{0.05}(FA_{0.92}MA_{0.08})_{0.95}Pb(I_{0.92}Br_{0.08})_3$ (1.4 M) was prepared by dissolving CsI, FAI, MAI, PbI_2, and $PbBr_2$ in a mixed solvent of DMF and DMSO (volume ratio 4:1). The perovskite films were fabricated using a two-step spin-coating process: 1000 rpm for 10 s followed by 5500 rpm for 30 s. During the second spin step, 150 μL of chlorobenzene was dropped onto the spinning substrate at 15 s. The films were then annealed at 100°C for 30 minutes. For the electron transport layer, a PCBM:C60 (1:1 by weight) solution in o-dichlorobenzene was spin-coated at 1000 rpm for 50 s. Subsequently, a $Zr(acac)_4$ solution in isopropanol was spin-coated on top at 4000 rpm for 40 s. Finally, a 100 nm Ag was thermally evaporated under a vacuum of 1.0×10^{-6} Pa. The active area of the devices was 0.105 cm^2.

Characterization

Current-voltage (*J-V*) measurements of the devices were tested using a source meter (Keithley 2635B) under illumination of solar simulator (Abet Sun 2000) at a standard irradiation of AM 1.5G (100 mW/cm^2). In stability test, *J-V* characteristics were recorded automatically at one hour interval using a source meter (Keithley 2635B) under illumination of white LED unit at a standard irradiation of AM 1.5G (100 mW/cm^2) in a nitrogen filled glove box at room temperature. In operational stability test, a constant biased voltage (0.94 V) at the maximum power point (MPP) was also applied. X-ray diffraction (XRD) patterns were taken using a diffractometer (Bruker D8 advance). Electron microscopic images were obtained on a Scanning electron microscopy (SEM) (Hitachi S4800) working at a 15 kV and a distant of ~8 mm with 20k multiplication using a secondary electron mode. The surface morphologies of the films were measured via atomic force microscope (AFM) (Nanocute, SII NanoTechnology). Steady state photoluminescence (PL) spectra were measured using a fluorescence spectrometer (Horiba Nanolog FL3-2iHR). Time-resolved photoluminescence (TRPL) spectra were obtained with ultrafast lifetime

spectrofluorometer (Horiba Delta flex). UV-Vis absorption spectra were taken with UV-Vis-NIR scanning spectrometer Shimadzu UV-3101PC. Ultraviolet photoemission spectroscopy (UPS) measurement was measured with an angle-resolved photoemission spectrometer (VG Scienta R4000 energy analyzer) using a monochromatic He I light source ($h\nu$ = 21.22 eV) under a sample bias of -5 V. X-ray photoelectron spectroscopy (XPS) was tested via X-ray photoelectron spectrometer (Thermo escalab 250Xi). Infrared spectra were obtained via Fourier transform infrared spectrometer (FT-IR) (Nicolet IS 10). Impedance of the materials was evaluated using an AC impedance analyzer (Solartron 1260) in frequency range from 1MHz to 0.1Hz at a voltage bias of 0.94V in the dark. Cyclic voltammetry (CV) measurements were performed using an electrochemical workstation (Model 660e), and cyclic curves at different scan rates were recorded after the electrolyte was connected.

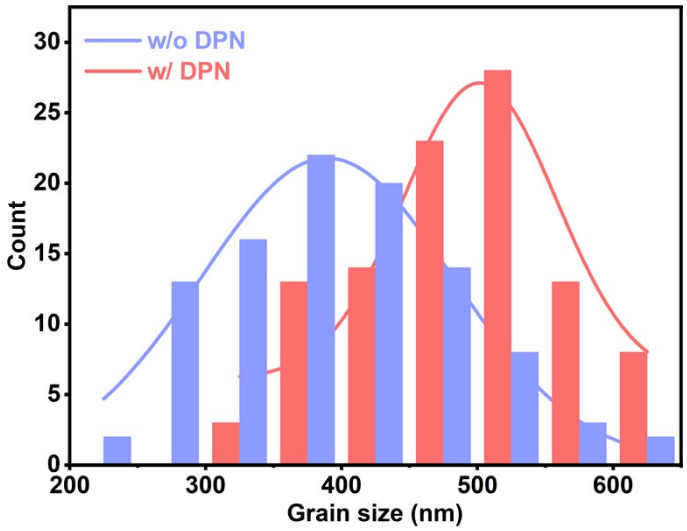

Figure S1. Grain size distribution graph from SEM.

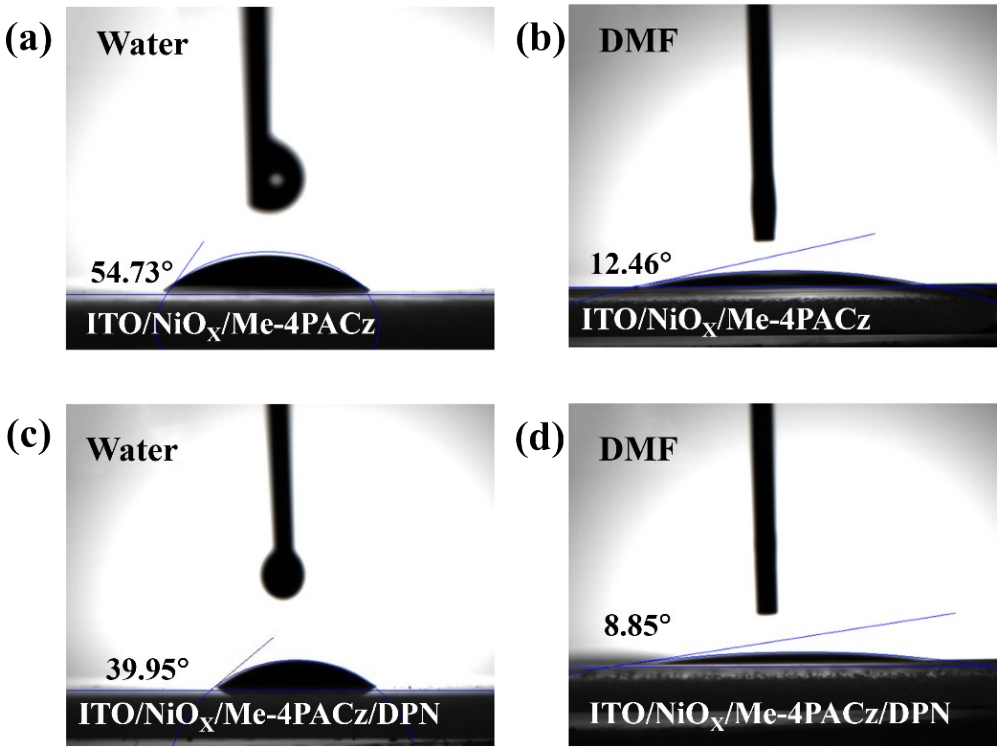

Figure S2. Contact angle measurements of water and DMF solvent droplets on the buried interfacial layers without and with DPN modification.

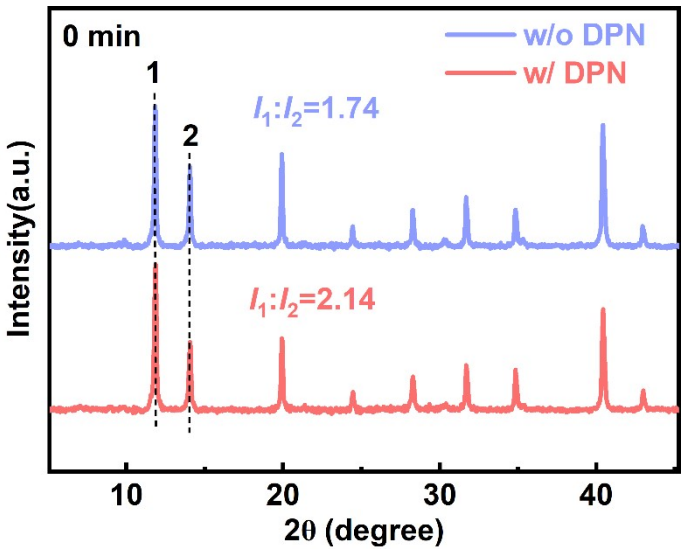

Figure S3. XRD patterns of perovskite films with and without DPN-modified before annealing.

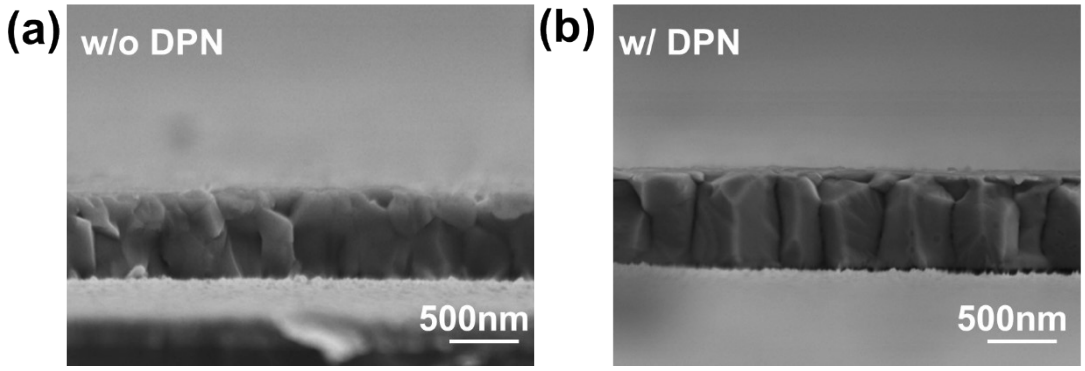

Figure S4. **(a, b)** Cross-SEM images of perovskite films deposited on ITO/ NiO_X/Me-4PACz and ITO/ NiO_X/Me-4PACz/DPN substrates, respectively.

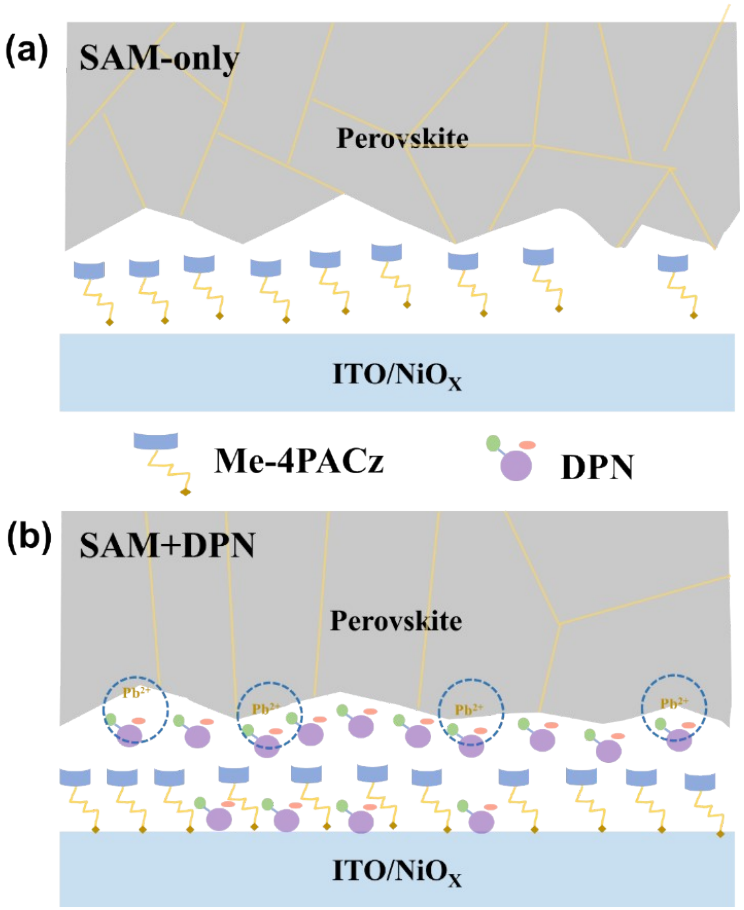

Figure S5. Schematic comparison of the buried interfaces with **(a)** SAM-only and **(b)** SAM+DPN modifications.

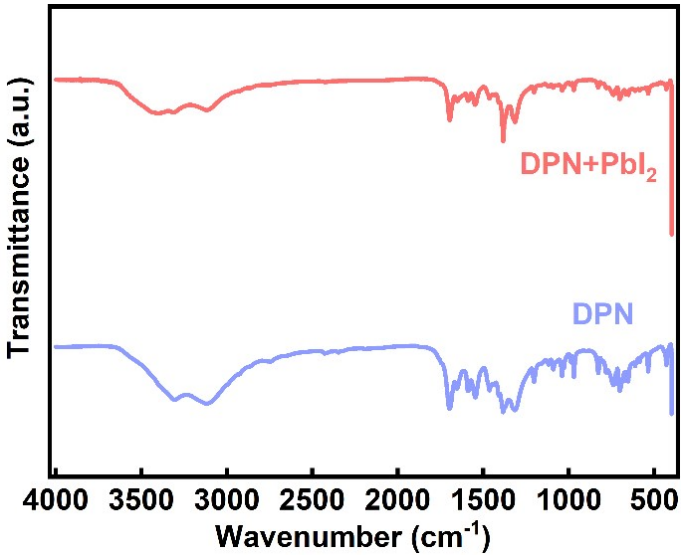

Figure S6. FTIR Spectra of DPN, and DPN+PbI_2 Mixture Powder.

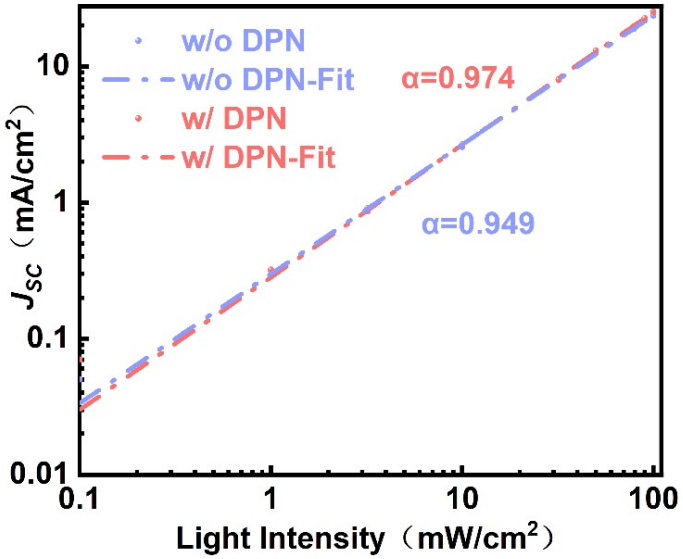

Figure S7. Linear relationship of J_{SC} with the natural logarithmic light intensity.

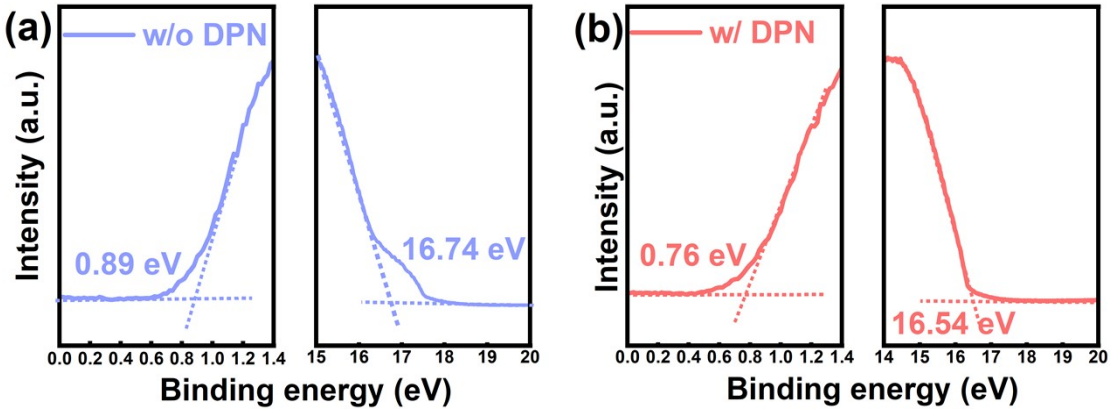

Figure S8. **(a)** UPS spectra of ITO/NiO_X/Me-4PACz film. (b) UPS spectra of ITO/NiO_X/Me-4PACz/DPN film.

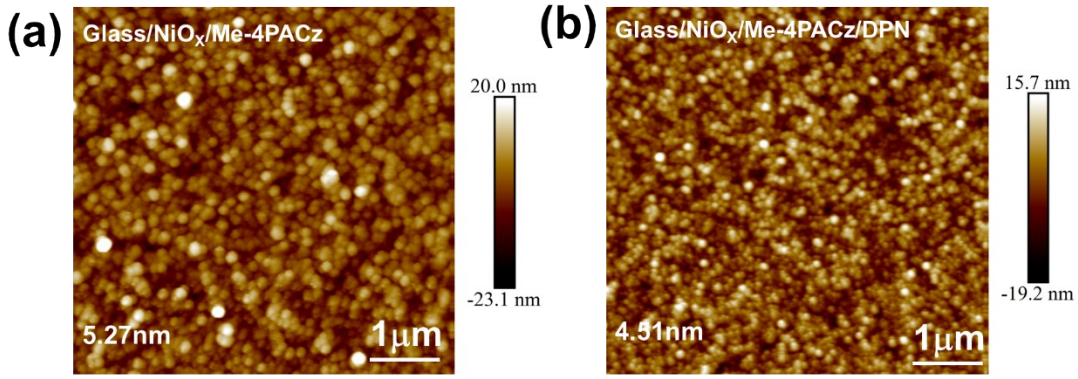

Figure S9. (a) AFM images of the top surface morphology of ITO/ NiO_X/Me-4PACz film. **(b)** AFM images of the top surface morphology of ITO/ NiO_X/Me-4PACz/DPN film.

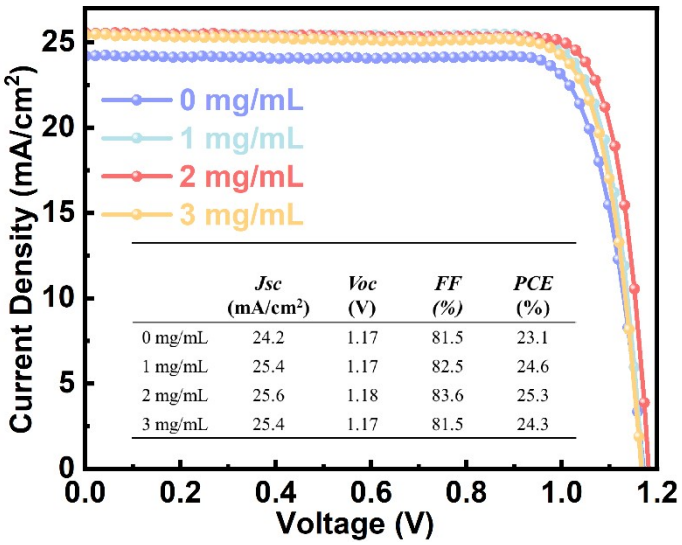

Figure S10. The *J-V* curves of the devices at different concentrations.

Table S1. Comparison of DPN with recently reported dual-site passivators.

Molecules	PLF[1]	Ph-Tz[2]	Co-BSA[3]	TFH[4]	DPN (this work)
Molecular structure	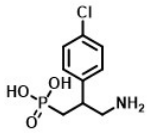	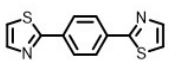	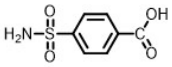	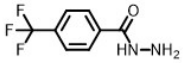	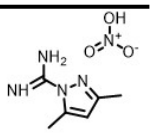
Interaction mechanism	Dual-sided bridging.	Synergistic dual-site coordination on thiazole ring.	Parallel-aligned molecules, simultaneous coordination with adjacent Pb^{2+} ions	Vertical orientation, strong dipole formation.	"Main-auxiliary" dual-site coordination.
Passivation effectiveness	Reduce defect density; Enhance crystallinity	Deep-level defect suppression; Lattice strain relaxation	Morphology optimization; Reduce trap state density	Suppress p-type self-doping; Improve charge extraction	Increase grain size; Optimize crystallization orientation; Release residual strain

Table S2. Fitting parameters for the TRPL measurements by using double-exponential model.

	τ_1 (ns)	A_1 (%)	τ_2 (ns)	A_2 (%)	τ_{avg} (ns)
Control	**110**	**4.18**	**2519**	**95.82**	**2418.3**
Target	**118**	**2.67**	**2900**	**97.33**	**2825.7**

Table S3. Initial performance parameters of the tested devices.

		J_{SC} (mA/cm^2)	V_{OC} (V)	FF (%)	PCE (%)
Operational Stability	w/o DPN	24.2	1.17	81.4	22.9
	w/ DPN	25.5	1.18	83.9	25.2
Storage Stability	w/o DPN	**23.9**	**1.17**	**81.7**	**22.8**
		24.1	1.17	81.0	22.8
		23.9	1.17	80.9	22.6
		23.7	1.17	81.9	22.7
		23.7	1.18	81.1	22.7
	w/ DPN	**25.4**	**1.18**	**83.4**	**25.0**
		25.4	1.18	83.0	24.9
		25.1	1.18	83.7	24.8
		25.2	1.18	83.5	24.8
		25.3	1.17	83.8	24.8

References

1. Z. Y. Wang, R. Su, Q. R. Zhang, J. W. Luo, X. P. Liu, D. Y. Luo, W. G. Xie and K. Chen, Adv. Funct. Mater., 2025, 35, 2501561.
2. D. Wang, Y. C. Li, W. J. Li, W. C. Pan, X. P. Liu, J. H. Wu, X. G. Guo and Q. H. Li, Angew. Chem. Int. Ed., 2025, 64, e202509529.
3. H. L. Huang, Y. S. Guo, W. Wang, Y. B. Wang, Z. W. Feng, J. J. Xu, H. Y. Zhang, Y. Ji, L. Li, X. Q. Wu, Y. T. Liu, Y. G. Peng, X. Li, Y. Fang, Y. R. Zhang, C. P. Huang, S. Y. Chen, W. C. Zhou, D. S. Tang, J. S. Sun, Y. Y. Li, B. Ding, J. Z. Liu, K. Weber, X. He, Y. Cui, N. Hu, H. L. Zhan, X. H. Zhang and J. Peng, Adv. Mater., 2025, 37, 2507918.
4. Y. Q. Bao, J. Zeng, Y. T. Xu, G. S. Xie, H. Hu, X. Lei, D. Wang, J. Y. Zhang, W. B. Peng, Z. X. Liu, P. D. Zhu, G. P. Qu, L. B. Qiu, L. Yan, Y. Zhang, X. Z. Wang and B. M. Xu, Adv. Energy Mater., 2025, 15, 2403186.